Effect of combined hole configuration on film cooling with and without mist injection

Tian, Ke; Wang, Jin; Liu, Chao; Baleta, Jakov; Yang, Li-Chen; Sunden, Bengt

EFFECT OF COMBINED HOLE CONFIGURATION ON FILM COOLING WITH AND WITHOUT MIST INJECTION

by

Ke TIAN[a], Jin WANG[a], Chao LIU[a], Jakov BALETA[b], Li YANG[a], and Bengt SUNDEN[c]*

[a] School of Energy and Environmental Engineering, Hebei University of Technology, Tianjin, China
[b] Department of Energy, Power Engineering and Environment,
Faculty of Mechanical Engineering and Naval Architecture, University of Zagreb, Zagreb, Croatia
[c] Department of Energy Sciences, Division of Heat Transfer, Lund University, Lund, Sweden

Turbine blades operate under a harsh environmental condition, and the inlet temperature of gas turbines is increasing with requirement of high engine efficiency. Some cooling schemes are adopted to prevent these blades from the thermal erosion of the hot mainstream. Film cooling technology is used widely and effectively in gas turbines. The coolant air is suppressed to the wall by the mainstream after jetting out of the film hole. A new hole configuration is first proposed to improve the film cooling characteristics in this paper. Comparison between a conventional cylindrical hole and a new combined hole is conducted by CFD, and effects of various blowing ratios and droplet sizes are also investigated. Results show that the combined hole configuration provides a wider coverage than that in the cylindrical hole configuration case at high blowing ratios (M = 1.0 and M = 1.5). In addition, the film cooling with mist injection also provides a significant enhancement on cooling performance especially for the combined hole case with a small droplet size (10^{-5} m).
Key words: film cooling, combined hole, CFD, blowing ratio, mist

Introduction

Improving the initial temperature is the most important way to increase the engine efficiency. However, it is limited by the melting temperature of the blade material. Film cooling technology has been widely used to provide protection for turbine blades. Film holes are arranged on the blade, and the coolant air separates the hot mainstream from the wall. The film cooling effectiveness is affected by many aspects. Grkovic [1] presented a mathematical model to conduct the calculation of the forces acting on the cooled turbine blades using the aerodynamic theory, and they found that the coolant flow had significant influence on the axial component of the resultant force. Kumar *et al.* [2] investigated the effect of three channel configurations on film cooling effectiveness, and they found that a better film cooling performance was obtained by using an internal channel with parabolic fin. Wang *et al.* [3] studied the effect of the upstream wake on the tip film cooling effectiveness using rods and delta wings. They found that the tip film cooling effectiveness was enhanced by the presence of the upstream wake.

1924

Tian, K., *et al.*: Effect of Combined Hole Configuration on Film Cooling…
THERMAL SCIENCE: Year 2018, Vol. 22, No. 5, pp. 1923-1931

Due to the simple machining process, cylindrical hole as a conventional configuration has been used in the film cooling technology for a long time. However, the coolant air cannot provide a wide coverage downstream the wall by using the cylindrical hole. Saumweber *et al.* [4] conducted experiments to investigate the film cooling performance of shaped holes at elevated free-stream turbulence conditions. They found that increasing turbulence level decreased the film cooling effectiveness for the shaped holes. Saumweber and Schulz [5] conducted a comparison of cylindrical and fan-shaped holes to investigate the effect of the free-stream on the cooling performance. They found that for diffused holes an increase in the turbulence intensity weakened the cooling performance. Nickol *et al.* [6] experimentally and numerically investigated three different hole shape configurations. They indicated that it was important to consider cooling designs in realistic environments. In addition, the blowing ratio and injection angle show significant impacts on film cooling effectiveness. Xie *et al.* [7] numerically studied heat transfer characteristics near the trailing edge of the turbine blade, and they found that the heat transfer coefficients could be enhanced significantly by increasing the blowing ratios. Bell *et al.* [8] measured film cooling effectiveness distributions by considering different hole geometries with or without a compound angle. They concluded that the configurations with a compound angle obtained a higher effectiveness than the simple configurations without a compound angle at high blowing ratios. Guo *et al.* [9] investigated the effect of the jet inclination angle and the blowing ratio on the flow field. They found that the strength of the vortices was reduced by decreasing the jet inclination angle.

Injecting droplets into the secondary flow is an effective scheme to obtain an enhanced cooling effectiveness due to evaporation of the water droplets. Oubella *et al.* [10] showed cooling enhancements during evaporation in a vertical channel using various liquid films. They found that the evaporation of the liquid films had significantly contribution to heat transfer. Li and Wang [11] investigated effect of mist injection on heat transfer, and various configurations with different compound angles of film holes were considered. Results showed that droplets with a small size had more evaporation, which provided a stronger cooling protection especially downstream the blade surface. Dhanasekaran and Wang [12] analyzed the influence of mist injection on the film cooling effectiveness in rotating conditions. They pointed out that the thermal protection decreased as the turbine was running at high speed. In addition, Wang *et al.* [13] numerically investigated the effects of deposition locations and heights on the film cooling effectiveness, and they concluded that the cooling performance had a significant improvement downstream the deposition by injecting mist. Wang *et al.* [14] investigated the effect of mist injection on the cooling performance. Results showed that the case without mist injection obtained better cooling performance by decreasing the height of the deposition. Based on the Lagrangian model, Zhou *et al.* [15] numerically simulated the cooling performance for three hole configuration cases with and without injection of water droplets. They found that the film cooling effectiveness both in the lateral direction and downstream the plate surface showed considerable enhancement as the mist cooling was taken into account.

In the present research, a combined hole configuration is first proposed, and the film cooling for the new configuration is compared to those of cylindrical hole configurations. The paper aims to investigate the effect of the extended outlet on film cooling effectiveness. In addition, cooling performance is analyzed under four blowing ratios, *i. e.*, 0.25, 0.5, 1.0, and 1.5. The film cooling with different droplet sizes (10 μm, 20 μm and 50 μm) are also taken into account.

Tian, K., *et al.*: Effect of Combined Hole Configuration on Film Cooling…
THERMAL SCIENCE: Year 2018, Vol. 22, No. 5, pp. 1923-1931
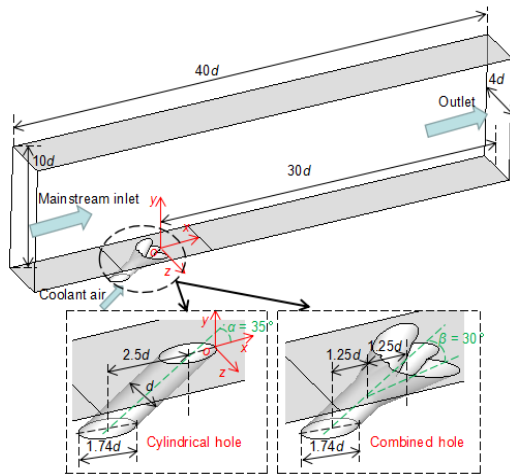
1925

Figure 1. Sketch of the computational domain

Numerical model

Figure 1 shows the 3-D computational model and two-hole configurations. The diameter, d, of the film hole is 8 mm. The dimensions of the computational domain are $40d \times 10d \times 4d$. Both the cylindrical and the combined hole configurations have the same injection angle of $\alpha = 35°$ in the middle section. In addition, the center distance in the vertical view of the two film holes is $2.5d$. In the combined hole cases, three cylindrical holes with the same diameter as the cylindrical hole cases are combined, and there is a distance of $1.25d$ between the beginning position of the hole combination and the inlet of the coolant flow. The combined hole has a lateral inclination angle, β, of 30°.

Boundary conditions

The temperature values of the mainstream and the coolant flow are set to 400 K and 300 K, respectively. Effects of four blowing ratios are investigated in this study. The inlet velocity of the mainstream is 10 m/s. The flow rate of the mist injection is $1.4 \cdot 10^{-5}$ kg/s. Side walls and other walls of the computational domain are set to symmetry boundary and no-slip conditions, respectively. More boundary conditions are shown in tab. 1.

Table 1. Boundary conditions

Zone	Type	Value
Mainstream inlet	Velocity-inlet	10 m/s, 400 K
Coolant flow inlet	Velocity-inlet	Air: $M = 0.25, 0.5, 1.0, 1.5$, 300 K Droplets: $1.4 \cdot 10^{-5}$ kg/s, 300 K
Outlet	Pressure-outlet	101325 Pa
Side walls	Symmetry	–
Other walls	No-slip	–

Governing equations

The standard k-ε turbulence model with enhance wall treatment is used to solve the steady-state Navier-Stokes equations in the present study. Moreover, the governing equations of mass, momentum, energy, the turbulent kinetic energy, k, and the turbulent dissipation rate, ε, are:

$$\frac{\partial}{\partial x_i}(\rho u_i) = S_{\mathrm{m}} \tag{1}$$

$$\frac{\partial}{\partial x_i}(\rho u_i u_j) = \rho \vec{g}_j - \frac{\partial P}{\partial x_j} + \frac{\partial}{\partial x_i}(\tau_{ij} - \rho \overline{u_i' u_j'}) + F_j \tag{2}$$

$$\frac{\partial}{\partial x_i}(\rho c_p u_i T) = \frac{\partial}{\partial x_i}\left(\lambda \frac{\partial T}{\partial x_i} - \rho c_p \overline{u_i' T'}\right) + \mu \Phi + S_{\mathrm{h}} \tag{3}$$

$$\frac{\partial}{\partial x_i}(\rho u_i k) = \frac{\partial}{\partial x_i}\left[\left(\mu + \frac{\mu_{\mathrm{t}}}{\sigma_k}\right)\frac{\partial k}{\partial x_i}\right] + G_{\mathrm{k}} - \rho \varepsilon \tag{4}$$

$$\frac{\partial}{\partial x_i}(\rho u_i \varepsilon) = \frac{\partial}{\partial x_i}\left[\left(\mu + \frac{\mu_t}{\sigma_\varepsilon}\right)\frac{\partial \varepsilon}{\partial x_i}\right] + C_{1\varepsilon}G_k\frac{\varepsilon}{k} - C_{2\varepsilon}\rho\frac{\varepsilon^2}{k} \tag{5}$$

where the source term S_m is the mass added to the continuous phase from the vaporization of the droplets. The source term F_j is the external body forces acting on the droplets, and the latent heat contributed from the droplets is included in the source term S_h. Moreover, the symmetric stress tensor is represented by τ_{ij}. $\mu\Phi$, and λ represent the dissipation heat and the effective heat conductivity. $\overline{\rho u_i' u_j'}$, $\overline{\rho c_p u_i' T'}$, and μ_t represent the Reynolds stresses, the turbulent heat fluxes and the turbulent viscosity, respectively.

The Newton's law is modified to analyze the discrete phase in this study, and it is described:

$$m_p\frac{dv_p}{dt} = F_d + F_g + F_o \tag{6}$$

where v_p is the vector velocity of the droplets, which can be affected by the hydrodynamic drag, F_d, the gravity, F_g, and other forces, F_o, in the flow field.

Evaporation of the water droplets occurs, when the water droplets encounter the mainstream. The vaporization rate is affected by the concentration difference between the surface and the air flow significantly, and the mass change rate of the water droplets is given:

$$\frac{dm_p}{dt} = \pi d^2 k_c(C_s - C_\infty) \tag{7}$$

where k_c, C_s, and C_∞ represent the mass transfer coefficient, the vapor concentration at the droplet surface and the vapor concentration of the bulk flow, respectively. More details about the mentioned equations can be found in [11, 16].

Grid independence and model validation

Figure 2 shows the meshes for the combined hole case. Unstructured grids are applied to the zone inside the film hole and near the outlet of the hole by using a multi-block method. For the computational domain with structured grids, there are 240, 120, and 32 grid cells meshed along x-, y- and z-directions, respectively. The cylindrical hole case has similar meshes to the combined hole case. The nearest wall cell has a value of $y^+ = 0.8$.

Figure 3a presents film cooling effectiveness on the centerline of the wall by using

Figure 2. Meshes

three grid cases (0.35, 1.70, and 2.60 million cells). The film cooling effectiveness, η, for the 0.35 million cell case has lower values than for the other cases, and there is a slight difference between the 1.70 and 2.60 million cell cases. Therefore, the case with 1.70 million cells was used to obtain all the results. Compared with the results of reference [8], the present simulation has almost overlapping temperature values at $x = 25d$ as shown in fig. 3b. For this paper, the same turbulence model and boundary conditions are employed to investigate the effect of different hole configurations on the film cooling by using ANSYS FLUENT 16.2.
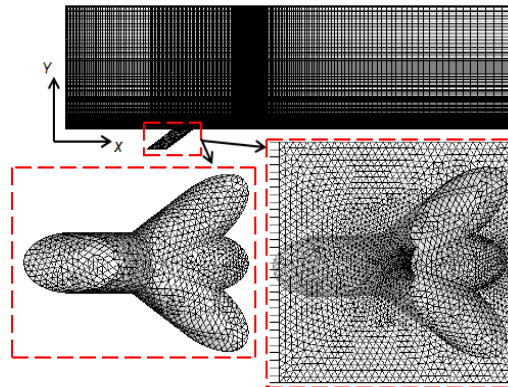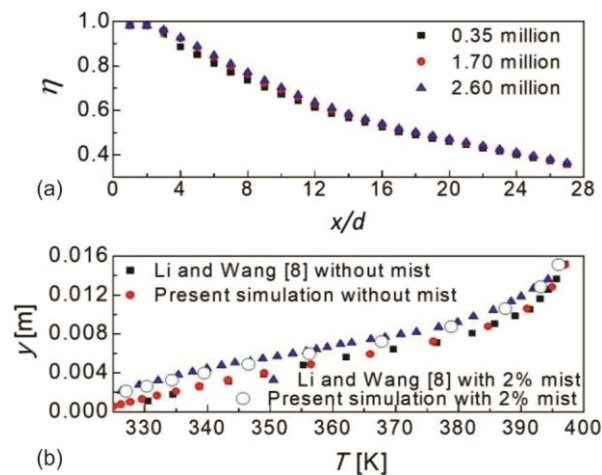
Tian, K., et al.: Effect of Combined Hole Configuration on Film Cooling…
THERMAL SCIENCE: Year 2018, Vol. 22, No. 5, pp. 1923-1931

1927

Figure 3. Grid independence and model validation

Results and discussion

Figure 4 shows streamlines and temperature contours on the middle section at blowing ratios of 0.25 and 1.0. The coolant air sticks to the downstream wall after the outlet of the holes. However, the velocity of the coolant flow is reduced by the large exit area of the combined hole case. Therefore, the cylindrical hole case has a lower wall temperature than the combined hole case, especially in the near-hole region. From the overall temperature distribution, the combined hole case has a better cooling performance than the cylindrical hole case at a high blowing ratio. The reason for this situation is that the coolant flow has a higher outlet velocity for the cylindrical hole, which results in a faster diffusion of the cooling coverage into the mainstream. However, for the combined hole, the velocity of the coolant flow decreases due to the lateral extension of the outlet, and the coolant flow at a high blowing ratio is pushed towards the wall.

Figure 5 shows the wall film cooling distributions for two-hole configurations at four blowing ratios. The film cooling effectiveness for the cylindrical hole case increases first and then decreases, as the blowing ratio increases. This is because diffusion of the coolant air is enhanced with the
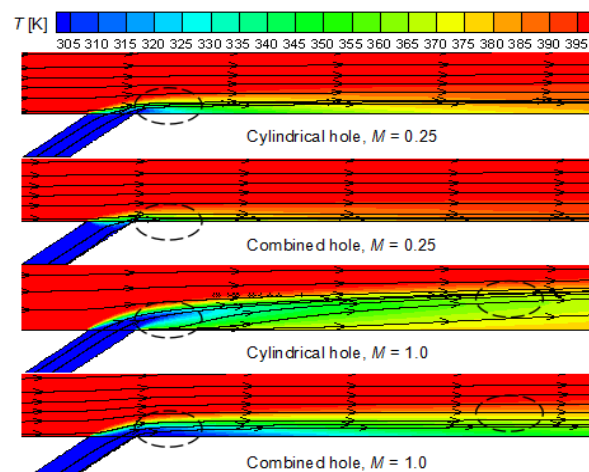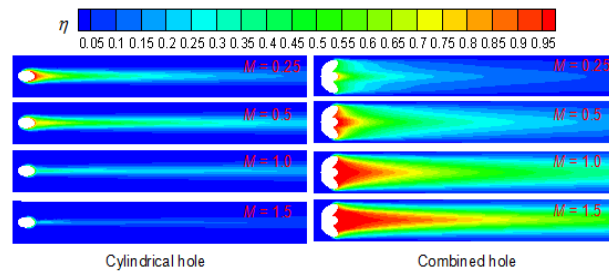

Figure 4. Streamlines and temperature contours on the middle sections at *M* = 0.25 and 1.0
(*for color image see journal web site*)

increase of the blowing ratio. The film cooling effectiveness for the combined hole configuration is improved by increasing the blowing ratio. Compared with the cylindrical hole case, the combined hole case shows a better lateral and streamwise (*x*-direction in fig. 1) cooling performance at high blowing ratios (*M* = 1.0 and 1.5). This indicates that the film cooling effectiveness can be improved by using a combined hole configuration.

For a comparison of two-hole configurations at four blowing ratios, the film cooling effectiveness downstream the wall is shown in fig. 6. However, a higher blowing ratio for the cylindrical hole shows a worse cooling effectiveness. For various blowing ratios, there is a significant difference of the film cooling effectiveness in the near-hole region. It is found that the film cooling effectiveness along the centerline sharply decreases for low blowing ratios (*M* = 0.25 and *M* = 0.5), whereas the cases at *M* = 1.0 and 1.5 show steady variations. The

combined hole configuration provides a better cooling effectiveness than the cylindrical case both at $M = 1.0$ and $M = 1.5$. The results show that the film cooling effectiveness downstream the wall is improved by increasing the blowing ratio.

Two downstream sections at $x = 3d$ and $15d$ are used to further analyze the lateral distribution of the film cooling effectiveness as shown in fig. 7. For the cylindrical hole case at $M = 1.5$, the maximum value of the film cooling effectiveness is lower than 0.2. However, the film cooling effectiveness for the combined hole case increases with the blowing ratio, and the maximum value on the centerline of the wall is 0.95. The combined hole case shows a higher lateral film cooling effectiveness compared to the cylindrical hole case at all the blowing ratios. Moreover, the coverage area of the lateral film cooling for the cylindrical hole case is smaller than for the combined hole case. For the two-hole configuration cases, the lateral film cooling effectiveness at $x = 15d$ is quantitatively analyzed as shown in fig. 7b. The lateral film cooling effectiveness at $x = 15d$ shows a similar trend to that at $x = 3d$. With the increase of the blowing ratio, the cooling performance for the cylindrical hole case increases first and then decreases, whereas the film cooling effectiveness for the combined hole case increases monotonically. It is concluded that the lateral film cooling effectiveness for the combined hole case is significantly improved by increasing the blowing ratio.
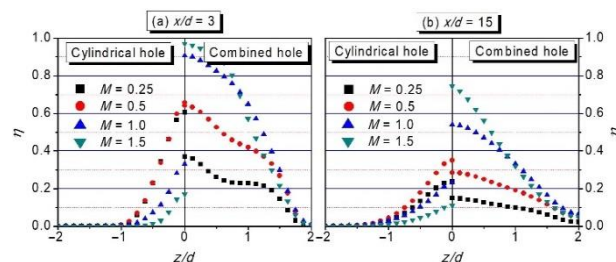

Figure 5. Film cooling effectiveness for two-hole configurations with different blowing ratios (*for color image see journal web site*)
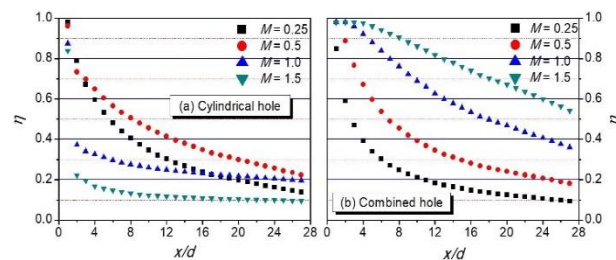
Figure 6. Film cooling effectiveness downstream the wall for two-hole configurations

Figure 7. Lateral film cooling effectiveness at $x = 3d$ and $x = 15d$ for two-hole configurations

From the results in fig. 7, it is evident that the cylindrical hole case has a larger coverage area at $x = 15d$ than at $x = 3d$. Moreover, for both the lateral and downstream film cooling effectiveness, the combined hole configuration provides higher values than those for the cylindrical hole configuration at high blowing ratios ($M = 1.0$ and 1.5). This is because the combined hole has an extended outlet, which separates more coolant air from the mainstream. More coolant flow diffuses into the mainstream. Lift force near the wall surface is weakened, which indicates that a stronger attachment ability is provided by using the combined hole configuration.

Tian, K., *et al.*: Effect of Combined Hole Configuration on Film Cooling…
THERMAL SCIENCE: Year 2018, Vol. 22, No. 5, pp. 1923-1931

1929

A parameter proposed in [17] is used to investigate the non-uniformity of the film cooling effectiveness distribution. This parameter, D_n, is calculated:

$$D_n = \frac{\sqrt{\sum_{i=1}^{N}(\eta_i - \eta_{avg})^2 / (N-1)}}{\eta_{avg}} \tag{8}$$

where η_i is the film cooling effectiveness of the grid node i on the wall and η_{avg} is the average value of the film cooling effectiveness on the specified surface.

Figure 8. Non-uniformity distribution, D_n, for two-hole configurations at various blowing ratios

Values of non-uniformity distributions of the film cooling effectiveness are shown in fig. 8. Compared with the cylindrical hole case, the combined hole case shows lower values of the non-uniformity distribution. This indicates that the combined hole configuration provides a more uniform film cooling distribution. The values of the non-uniformity distribution slightly decrease with an increase of the blowing ratio (except $M = 1.0$). This indicates that the most uniform distribution of the film cooling effectiveness can be obtained at a blowing ratio of 1.0, although increasing the blowing ratio usually provides a better cooling performance.
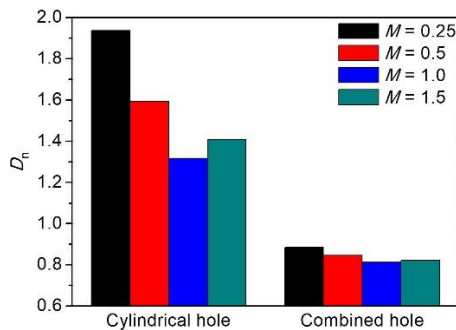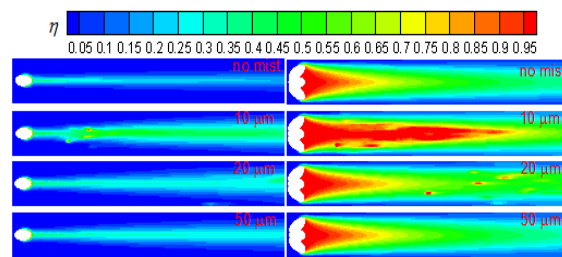

Figure 9. Film cooling effectiveness for two-hole configurations with different droplet sizes, $M = 1.0$
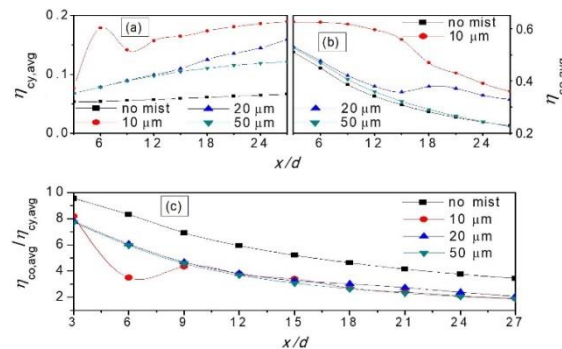

Figure 10. Lateral averaged film cooling effectiveness for the cases with different droplet sizes, $M = 1.0$

Figure 9 shows the adiabatic film cooling effectiveness for two-hole configuration cases with three droplet sizes, *i. e.*, 10, 20, and 50 μm. All the cases in this part are calculated at a blowing ratio of 1.0. It is found that the cooling performance for the mist injection cases has a significant improvement due to evaporation of the water droplets. This is because more heat flux is taken away by vaporization after the water droplets flying a distance along the wall surface. From the results, the film cooling effectiveness downstream the wall decreases with an increase of the droplet size. The droplets with a smaller size have a larger specific surface area, which results in a faster vaporization and wider diffusion. In addition, for the cases with a mist injection, the lateral film cooling effectiveness is gradually improved downstream the wall. Compared with the cylindrical hole case, the combined hole case shows a better cooling performance especially in the lateral direction.

Effect of various droplet sizes on the lateral averaged film cooling effectiveness is investigated for two-hole configurations as shown in fig. 10. Compared with other cases, the 10 μm cases with both the combined and cylindrical holes obtain the highest lateral averaged values of the film cooling effectiveness.

To investigate the effect of various hole configurations on the film cooling quantitatively, fig. 10(c) shows lateral averaged ratios of the film cooling effectiveness ($\eta_{co,avg}/\eta_{cy,avg}$). For these ratios ranging from 2 to 10, it is indicated that the combined hole provides a significant enhancement on the film cooling effectiveness, especially for no mist cases.

Conclusions

The CFD was used to investigate cooling performance in a channel by considering two-hole configurations, *i. e.*, combined and cylindrical hole configurations. The flow distributions and the film cooling effectiveness were analyzed along both the lateral and streamwise directions.

The conclusions for this paper can be summarized as follows.
- The film cooling effectiveness for the cylindrical hole case decreases with the increase of the blowing ratio, whereas that for the combined hole case increases by increasing the blowing ratio.
- For the cylindrical hole case, a better cooling performance downstream the wall is obtained at low blowing ratios ($M = 0.25$ and 0.5) compared to the combined hole case, however, the coolant air diffuses into the mainstream quickly at high blowing ratios due to the increase of the lift force, and compared to the cylindrical hole case, the combined hole configuration separates more coolant air from the mainstream due to presence of an extended outlet.
- The film cooling with mist injection shows a significant enhancement of the cooling effectiveness, especially for the cases with a small size of water droplets and or the blowing ratio of 1.0, the combined hole case with mist injection shows better cooling protections both in the lateral and downstream directions.

Acknowledgment

Nomenclature

c_p – specific heat, [Jkg^{-1}K^{-1}]
D_n – non-uniformity distribution, [–]
d – diameter of film hole, [m]
F – force, [N]
k – turbulence kinetic energy, [m^{2}s^{-2}]
k_c – mass transfer coefficient, [ms^{-1}]
M – blowing ratio [$= (\rho u)_c/(\rho u)_g$], [–]
m – mass, [kg]
P – pressure, [Nm^{-2}]
S – source term, [–]
T – temperature, [K]
u – stream-wise velocity component, [ms^{-1}]
x, y, z – co-ordinates, [m]

Greek symbols

α – inclination angle, [°]
β – lateral inclination angle, [°]
ε – turbulence dissipation rate, [m^{2}s^{-3}]
η – adiabatic film cooling effectiveness,
       [$= (T_g - T_{aw})/(T_g - T_c)$], [–]
λ – thermal conductivity, [Wm^{-1}K^{-1}]
μ – dynamic viscosity, [kgm^{-1}s^{-1}]
ρ – density, [kgm^{-3}]
σ_k – turbulent Prandtl number
τ – stress tensor, [kgm^{-1}s^{-2}]

Subscripts

avg – averaged value
aw – adiabatic wall
c – coolant jet
co – combined hole
cy – cylindrical hole

Tian, K., *et al.*: Effect of Combined Hole Configuration on Film Cooling…
THERMAL SCIENCE: Year 2018, Vol. 22, No. 5, pp. 1923-1931

1931

g	− hot gas	s	− droplet surface
n	− number	∞	− far away from droplet
p	− droplet		

References

[1] Grkovic, V. R., A Method for Calculation of Forces Acting on Air Cooled Gas Turbine Blades Based on the Aerodynamic Theory, *Thermal Science*, *17* (2013), 2, pp. 547-554

[2] Kumar, M., *et al*., Conjugated Heat Transfer Analysis of Gas Turbine Vanes Using MacCormack's Technique, *Thermal Science*, *12* (2008), 3, pp. 65-73

[3] Wang, J., *et al*., Effect of Upstream Wake on Passage Flow and Tip Film Cooling Characteristics, *Proceedings*, ASME Turbo Expo 2012: Power for Land, Sea and Air, Copenhagen, Denmark, 2012, pp. 1381-1387

[4] Saumweber, C., *et al*., Free-Stream Turbulence Effects on Film Cooling with Shaped Holes, *ASME Turbo Expo 2002: Journal of Turbomachinery*, *17* (2002), 2, pp. 41-49

[5] Saumweber, C., Schulz, A., Free-Stream Effects on the Cooling Performance of Cylindrical and Fan-Shaped Cooling Holes, *ASME Turbo Expo 2008: Power for Land, Sea, and Air*, *134* (2008), 6, pp. 879-891

[6] Nickol, J. B., *et al*., Unsteady Heat Transfer and Pressure Measurements on the Airfoils of a Rotating Transonic Turbine with Multiple Cooling Configurations, *ASME Turbo Expo 2016: Turbomachinery Technical Conference and Exposition*, *139* (2017), 9, V05AT13A027

[7] Xie, Y. H., *et al*., Numerical Study on Film Cooling and Convective Heat Transfer Characteristics in the Cutback Region of Turbine Blade Trailing Edge, *Thermal Science*, *20* (2016), Suppl. 3, pp. S643-S649

[8] Bell, C. M., *et al*., Film Cooling from Shaped Holes, *ASME Journal of Heat Transfer*, *122* (2000), 2, pp. 224-232

[9] Guo, X., *et al*., Large-Eddy Simulations of Film Cooling Flows, *Computers and Fluids*, *35* (2006), 6, pp. 587-606

[10] Oubella, M., *et al*., Numerical Study of Heat and Mass Transfer during Evaporation of a Thin Liquid Film, *Thermal Science*, *19* (2015), 5, pp. 1805-1819

[11] Li, X., Wang, T., Simulation of Film Cooling Enhancement with Mist Injection, *Journal of Heat Transfer*, *128* (2006), 6, pp. 509-519

[12] Dhanasekaran, T. S., Wang, T., Simulation of Mist Film Cooling on Rotating Gas Turbine Blades, *ASME Turbo Expo 2009: Power for Land, Sea, and Air*, *134* (2012), 1, pp. 395-408

[13] Wang, J., *et al*., Effects of Deposition Locations on Film Cooling with and without a Mist Injection, *Numerical Heat Transfer Part A: Applications*, *70* (2016), 10, pp. 1072-1086

[14] Wang, J., *et al*., Effects of Surface Deposition and Droplet Injection on Film Cooling, *Energy Conversion and Management*, *125* (2016), Oct., pp. 51-58

[15] Zhou, J., *et al*., CFD Analysis of Mist/Air Film Cooling on a Flat Plate with Different Hole Types, *Numerical Heat Transfer Part A: Applications*, *71* (2017), 11, pp. 1123-1140

[16] Wilcox, D. C., *Turbulence Modeling for CFD*, DCW Industries Inc., La Canada Flintridge, Cal., USA, 2006

[17] Wang, J., *et al*., Investigations of Film Cooling and its Non-Uniform Distribution for the Conjugate Heat Transfer Passage with a Compound Inclined Angle Jet, *Numerical Heat Transfer Part A: Applications*, *69* (2016), 1, pp. 14-30